


# Detection of an electron beam in a high density plasma via an electrostatic probe

Stephen Majeski<sup>1</sup>, Jongsoo Yoo<sup>2</sup> , Stewart Zweben<sup>2</sup> and Masaaki Yamada<sup>2</sup>

<sup>1</sup>Rensselaer Polytechnic Institute, 110 Eighth Street, Troy, NY 12180, United States of America

<sup>2</sup>Princeton Plasma Physics Laboratory, Princeton, NJ 08543, United States of America

E-mail: [jyoo@pppl.gov](mailto:jyoo@pppl.gov)

Received 5 December 2017, revised 19 March 2018

Accepted for publication 10 April 2018

Published 8 May 2018



CrossMark

## Abstract

An electron beam is detected by a 1D floating potential probe array in a relatively high density ( $10^{12}$ – $10^{13}$  cm<sup>-3</sup>) and low temperature ( $\sim 5$  eV) plasma of the Magnetic Reconnection Experiment. Clear perturbations in the floating potential profile by the electron beam are observed. Based on the floating potential profile and a current balance equation to the probe array tips, the effective width of the electron beam is determined, from which we determine the radial and toroidal beam current density profiles. After the profile of the electron beam is specified from the measured beam current, we demonstrate the consistency of the current balance equation and the location of the perturbation is also in agreement with field line mapping. No significant broadening of the electron beam is observed after the beam propagates for tens of centimeters through the high density plasma. These results prove that the field line mapping is, in principle, possible in high density plasmas.

Keywords: electron beam detection, floating potential, field line mapping

(Some figures may appear in colour only in the online journal)

## 1. Introduction

The electron beam has often been used to trace the vacuum magnetic field line topology in plasma devices [1–3]. Since the motion of the electron beam is dominated by the parallel component, field line mapping can be achieved by detecting the light from interaction between the electron beam and the low-density background gas via a fast camera. In a high density plasma, however, this method is not viable, as background light becomes dominant over the light from the electron beam. The measurement of the field line topology in a high density plasma is important for some laboratory experiments such as studies of magnetic reconnection [4]. Although these measurements are usually done by *in situ* magnetic probes [5, 6], the direct measurement of the 3D field line topology or stochasticity is limited by technical difficulties such as limited number of digitizer channels and limited frequency response of magnetic pickup coils.

Here, an alternative method of locating an electron beam is presented, which can be potentially used to directly measure the field line topology in a high density plasma. In

particular, a 1D floating potential ( $V_f$ ) probe array with 25 tips has been used to measure the perturbation of the floating potential by a 200 eV (200 V accelerating potential) electron beam in a high density ( $10^{12}$ – $10^{13}$  cm<sup>-3</sup>) plasma with an electron temperature of about 5 eV. The beam perturbs the floating potential after traveling about 0.20 m along the magnetic field line. In section 2, a short description of the apparatus is presented. In sections 3 and 4, measurements of the floating potential perturbation are compared with theoretical values. Finally, we discuss a possible application of this method to the measurement of the magnetic field line topology.

## 2. Methods

The experimental campaign reported here was performed in the Magnetic Reconnection Experiment (MRX) at the Princeton Plasma Physics Laboratory [5]. MRX has a cylindrical vacuum vessel with a radius of about 0.76 m. In MRX, the plasma is inductively generated by two sets of internal coils.

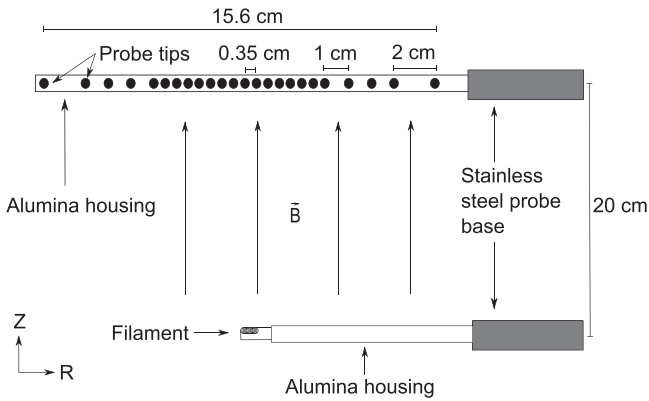


**Figure 1.** Schematic for the experimental setup. An electron beam generated by a tungsten filament travels about 0.20 m along the magnetic field and reaches a floating potential ( $V_f$ ) probe array. The filament is radially located at the center of the floating potential probe, 0.62 m from the center of MRX. The 1D profile of  $V_f$  is measured to determine the location of the electron beam as well as the profile of the electron beam density. The magnitude of the  $V_f$  perturbation is compared with theoretical values. The magnetic field is generated by external coils, which produces straight field lines.

The electron density is relatively high, which is typically  $1\text{--}10 \times 10^{13} \text{ cm}^{-3}$  and the electron temperature is relatively low, ranging from 3 to 15 eV. Although MRX has a relatively complex magnetic geometry at the center of the device, the field line is straight near the wall where all the measurements have been carried out. This straight field line has been confirmed by detecting light from the electron beam without a background plasma, as well as with magnetic probes during discharges. As the vessel is cylindrical, where necessary we will make use of the cylindrical coordinate system ( $R, \theta, Z$ ). Note that due to the scale of the experiment compared to that of MRX,  $\theta$  will be in units of length, and is used to indicate the direction normal to the  $R$ – $Z$  plane.

To detect the electron beam in a high density plasma, a floating potential probe array was constructed. The layout of the 25 probe tips is shown in the top part of figure 1. The maximum resolution along the radial ( $R$ ) direction is 0.35 mm and the total coverage of the probe is 15.6 cm. The probe array is inserted into the MRX chamber radially, perpendicular to the axial magnetic field generated by internal and external coils, with the tips facing the filament. As shown in figure 1, the probe array is separated from the electron beam source by 0.20 m along the magnetic field. The electrostatic probe contains a number of points where two probe tips are located on either side of the center line of the probe. These tips are 2 mm apart and the value of  $V_f$  at these two tips was averaged to imitate a single measurement point. Due to the effective width of the beam and radial variation of  $V_f$  over 1 mm, we assume here that the difference between  $V_f$  along the center line of the probe and at the measurement points is small. The filament is a tungsten filament, with a coil diameter of 1.3 mm, and a wire diameter of 0.1 mm. The length of the filament in the radial direction is 1.3 cm, and it contains approximately 47 turns in that length.

The electron beam is generated by an emitting tungsten filament, biased a few hundred volts negative with respect to

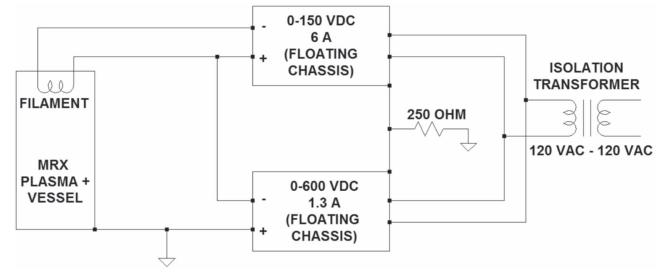


**Figure 2.** Schematic for the electron beam apparatus. The filament, a 1 mm diameter tungsten coil, is heated with a high-current ( $\sim 4$  A) and low-voltage power supply. Then, the filament is biased at a high voltage (typically 200 V) with respect to the machine ground with an additional high-voltage power supply. The most of the voltage drop occurs across the Debye sheath to accelerate electrons, generating electron beams. The beam current is measured by a Pearson current meter which detects the difference in current from the wires going to and from the filament.

the stainless steel vacuum vessel of MRX. Figure 2 shows the schematic for the electron beam system in MRX. The filament current is supplied by a high-current power supply, while the bias voltage for the electron beam is provided by a high-voltage power supply. A typical current through the filament without a plasma is about 4 A. Since the bias voltage is much larger than the plasma potential at the filament, the beam energy is mostly determined by the bias voltage. The beam electrons stream to the floating potential probe array and eventually to the chamber along the open field lines. The magnetic field strength at the beam location is about 500 Gauss, enough to magnetize the beam electrons. The radial location of the filament is  $R = 0.62$  m; under this straight field line geometry, the beam will arrive at the floating potential probe with the central radial location of  $R = 0.62$  m. The electron density and temperature of the background plasma are measured by a triple Langmuir probe [7]. The probe is placed at the midpoint of the beam path, but separated azimuthally by 4 cm to avoid direct interaction with the electron beam.

### 3. Results

Figure 3 shows time profiles of the electron density ( $n_e$ ) and electron temperature ( $T_e$ ), measured by the triple Langmuir probe. Data is averaged over 50 discharges and typical errors associated with these measurements are less than 10%, especially after 400  $\mu\text{s}$ . The plasma density rapidly increases after the bulk plasma is created at 214  $\mu\text{s}$ . During this time, the ratio of the beam electron density ( $n_b$ ) to the background electron density ( $n_e$ ) is small ( $< 10^{-3}$ ). At these times ( $< 400 \mu\text{s}$ ), the perturbation is relatively small ( $\sim 1$  V) and is hard to be quantified due to effects from the plasma formation at  $t = 214 \mu\text{s}$ . After 400  $\mu\text{s}$ , the ratio is typically about  $10^{-3}$ , so the perturbation from the electron beam can be clearly detected by the  $V_f$  probe array. The amount of the floating potential perturbation can be easily controlled by changing the beam ratio ( $n_b/n_e$ ). Here, the maximum value of  $n_b/n_e$  is less than 1%, such that instabilities driven by a strong electron

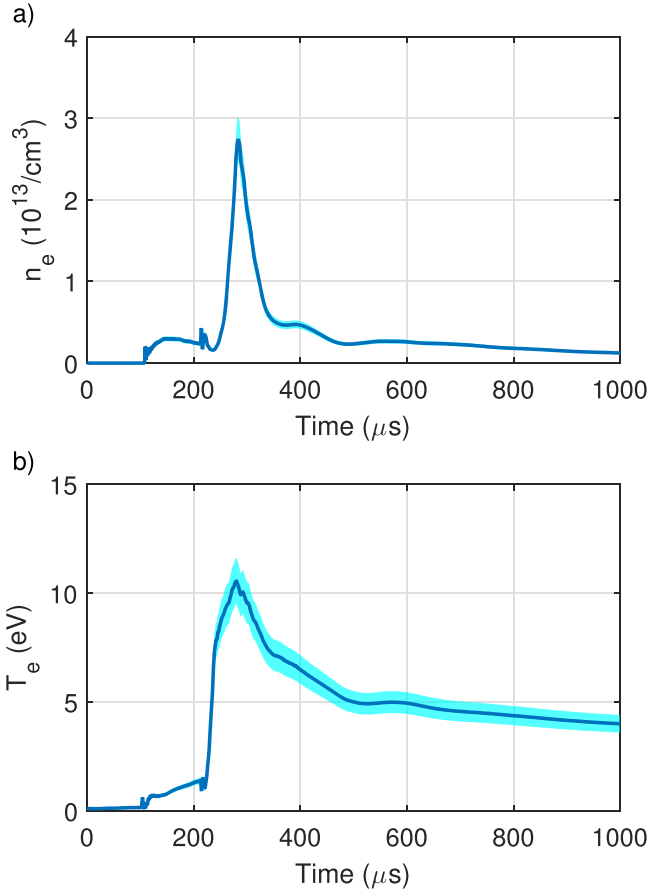


**Figure 3.** Time evolutions of the electron density (a) and temperature (b). Both profiles are averaged over 50 discharges in MRX. The floating potential profile data presented in this manuscript is obtained at 550, 650, 750, and 950  $\mu\text{s}$  when the plasma temperature and density are stable with typical values of 4–5 eV and  $2 \times 10^{12} \text{ cm}^{-3}$ , respectively. Errors associated with Langmuir probe measurements are indicated by the cyan color.

beam [8, 9] are not expected to exist in this plasma. After 400  $\mu\text{s}$ , the electron density is less than  $1 \times 10^{13} \text{ cm}^{-3}$  and the typical electron temperature is about 5 eV, as shown in figures 3(a) and (b), respectively.

An example of the floating potential profile created by the floating probe array is presented in figure 4. It displays the profile for various beam probe conditions: a cold biased filament, a hot unbiased filament, a cold unbiased filament, and a hot biased filament. This is shown in order to display the effects of the individual functions of the beam system on  $V_f$ . The perturbation due to the beam can be clearly observed at approximately 0.62 m, while the presence of the beam probe appears to have little effect on the floating potential downstream. Note that the central radial location of the  $V_f$  perturbation is the same as the location of the filament ( $R = 0.62 \text{ m}$ ), which is consistent with the straight field line geometry. Thus, the field line mapping via the floating potential measurements is possible in this relatively high-density plasma.

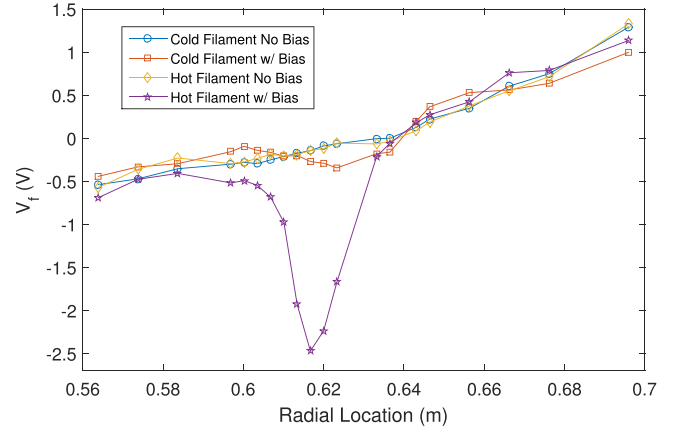


**Figure 4.** Radial  $V_f$  profiles for a cold biased filament, a hot unbiased filament, a cold unbiased filament, and a hot biased filament. This demonstrates the individual effects of the different functions of the electron beam system on  $V_f$ , as well as showing what the radial  $V_f$  profile looks like in the absence of the beam. The data for all profiles shown above was collected after 400  $\mu\text{s}$ , when the density and temperature have stabilized.

#### 4. Discussion

The amount of  $V_f$  perturbation depends on the ratio of the beam and plasma densities ( $n_b/n_e$ ), the electron temperature ( $T_e$ ), and the beam energy. In the absence of a beam,  $V_f$  can be found by equating the electron current and the ion saturation current drawn by a  $V_f$  probe array tip [10]:

$$Aen_e \sqrt{\frac{kT_e}{2\pi m_e}} \exp\left[\frac{e(V_f - V_p)}{kT_e}\right] = \exp\left(-\frac{1}{2}\right) Aen_e C_s = I_{\text{sat}}, \quad (1)$$

where  $A$  is the area of the probe tip,  $m_e$  is the electron mass,  $C_s \equiv \sqrt{kT_e/m_i}$  is the sound velocity with the ion mass,  $m_i$ ,  $e$  is the electron charge,  $V_p$  is the plasma potential, and  $I_{\text{sat}}$  is the ion saturation current. From equation (1), the floating potential without an electron beam is

$$\begin{aligned} V_f - V_p &= \frac{kT_e}{e} \ln \left[ \exp\left(-\frac{1}{2}\right) \sqrt{\frac{2\pi m_e}{m_i}} \right] \\ &= -(3.3 + 0.5 \ln \mu) \frac{kT_e}{e}, \end{aligned} \quad (2)$$

where  $\mu = m_i/m_p$  is the ratio of the ion mass to the proton mass,  $m_p$ .

With the presence of an electron beam, the beam current to the probe,  $I_b = -en_b A_p \langle v_b \rangle$ , has to be added to the left-hand side of equation (1), which makes the floating potential decrease. Here,  $\langle v_b \rangle$  is the average beam velocity, and  $A_p$  is the probe area seen by the electron beam. Due to the beam-plasma interaction, it is unlikely that all of beam electrons maintain the initial velocity, so  $\langle v_b \rangle$  is a unknown quantity. For our conditions, the Larmor radius of the beam electrons is on average comparable to the size of the probe array tips, so we set  $A_p = A$ . If equation (1) with  $I_b$  added is solved for  $V_f$  and equation (2) is subtracted, the change in the floating

potential ( $\Delta V_f$ ) is given by [11]

$$\Delta V_f = \frac{kT_e}{e} \ln \left[ 1 + \exp \left( \frac{1}{2} \frac{J_b A_p}{en_e A C_s} \right) \right] = \frac{kT_e}{e} \ln \left[ 1 + \frac{I_b}{I_{\text{sat}}} \right], \quad (3)$$

where  $J_b = -en_b \langle v_b \rangle$  is the current density of the beam.

To determine the effective width of the profile in the  $\theta$  direction, the current density profile in the  $R$ - $\theta$  plane of the electron beam,  $J_b(R, \theta)$ , has to be specified. Here, it is assumed to be Gaussian in both directions:

$$J_b(R, \theta) = \frac{j_0}{2\pi\sigma_R\sigma_\theta} \exp \left( -\frac{(R-a)^2}{2\sigma_R^2} - \frac{\theta^2}{2\sigma_\theta^2} \right), \quad (4)$$

where  $a = 0.62$  m is the radial location of the beam and the  $\theta$  beam location is on the radial axis of the probe, which we have set to 0 mm.  $\sigma_R$  is the effective width of the beam in the radial direction,  $\sigma_\theta$  is the effective width in the  $\theta$  direction, and  $j_0$  is the normalization factor. The effective radial width of the beam,  $\sigma_R$  is determined to be 7.7 mm from the averaged full width at half maximum (FWHM) of floating potential profiles (FWHM =  $2\sigma\sqrt{2\ln 2}$ ). This width agrees well with the length of the filament and therefore the emitting surface along the radial direction, which is about 13 mm. This indicates that any broadening of the beam is minimal. The normalization factor,  $j_0$  is determined by the following constraint:

$$I_m - \exp \left( -\frac{1}{2} \right) A_f en_e C_s = 2 \iint J_b(R, \theta) dR d\theta = 2j_0, \quad (5)$$

where  $I_m$  is the measured beam current. It should be noted that the contribution from the ion saturation current drawn by the filament is subtracted from the total current in order to obtain the true beam current. The factor of 2 on the right-hand side comes from the fact that the electron beam propagates along both  $+Z$  and  $-Z$  directions. By solving equation (5) for  $j_0$ , setting  $a = 0$  in equation (4), and entering this value for  $J_b(R, \theta)$  into equation (3), we solve for  $\sigma_\theta$  given  $\Delta V_f$  and plasma parameters. We found  $\sigma_\theta$  to be on average 1.6 mm.

The beam density can be also approximated under the assumption of the isotropic beam electron emission from the filament and minimal beam-plasma interaction. In this case, we can assume the average parallel velocity is  $\langle v_b \rangle \approx (2/\pi)\sqrt{2eE_b/m_e}$ , where  $E_b$  is the bias voltage for the electron beam. With this value, the beam density profile can be determined by  $n_b = -J_b/(e\langle v_b \rangle)$ , which typically gives  $n_b$  on the order of  $10^9$  cm $^{-3}$ .

Figure 5 shows an example of the measured floating potential profile with the presence of an electron beam for  $\theta = 0$ . It shows a clear potential well centered near  $R = 0.62$  m. The red curve denotes the potential profile calculated by equation (3) after  $J_b(R, \theta)$  is determined from the measured beam current ( $I_m = 0.45$  A in this case). The background electron density is  $3 \times 10^{12}$  cm $^{-3}$  and temperature is 4.5 eV, which are measured by the reference Langmuir probe. These two profiles are in good agreement except the slight positive slope in the measured profile, which is caused by a remnant

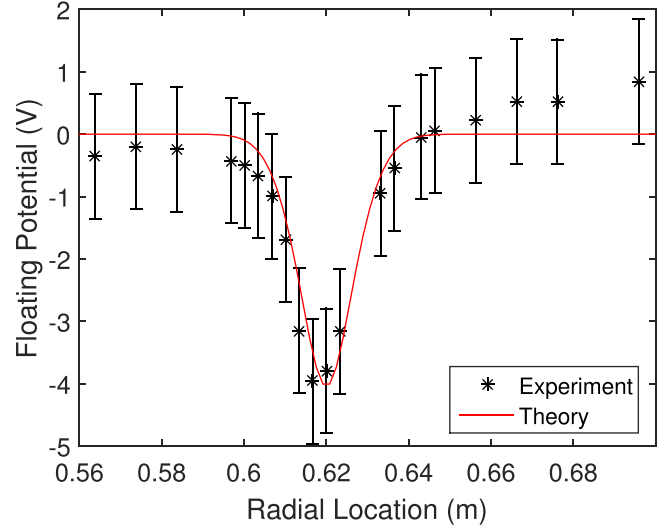


**Figure 5.** Example of the radial floating potential profile. Black asterisks are measured floating potentials, while the red curve is the floating potential profile calculated from equation (3). The radial beam current density profile,  $J_b(R)$  is determined from the measured beam current ( $I_m = 0.45$  A) and the beam radial ( $\sigma_R = 7.7$  mm) and azimuthal ( $\sigma_\theta = 1.6$  mm) widths, we have also set  $\theta = 0$ . This data was collected at 750  $\mu$ s with background electron density  $n_e = 3 \times 10^{12}$  cm $^{-3}$  and electron temperature  $T_e = 4.5$  eV, which were measured by a reference Langmuir probe. The filament bias here is  $-200$  V. The error present in the probe array measurements are estimated from the magnitude of fluctuations in floating potential ( $1$  V). The net slope in the experimental profile is caused by a remnant electric field from the plasma formation, this is confirmed by the resulting profile with no bias applied to the filament.

electric field from the plasma formation [12]. As shown in figure 4, the slope exists even without the beam. This agreement justifies the process of determining the local beam current density. We repeated the profile measurement under different plasma conditions, but there is no noticeable broadening of the electron beam if  $n_b/n_e < 1 \times 10^{-3}$ .

The above formulation assumes a weak beam-plasma interaction while the electron beam travels to the floating potential probe. Negligible broadening of the electron beam supports this idea. A completely different explanation, however, is possible; the electron temperature increase via a strong beam-plasma interaction can lead to the floating potential perturbation. From equation (2), the floating potential can decrease with respect to  $V_p$ , if the local electron temperature  $T_e$  increases. The plasma potential may also be perturbed [13] but the change is expected to be minimal under the assumption of the strong beam-plasma interaction and small  $n_b/n_e$ . Assuming an isotropic electron distribution and negligible cross-field heat transport, the electron temperature increase by the electron beam is given by

$$\frac{3}{2} \frac{n_e k \Delta T_e}{e} \approx n_b E_b. \quad (6)$$

If the electron beam only increases the parallel electron temperature, the factor  $3/2$  and  $\Delta T_e$  should be replaced by

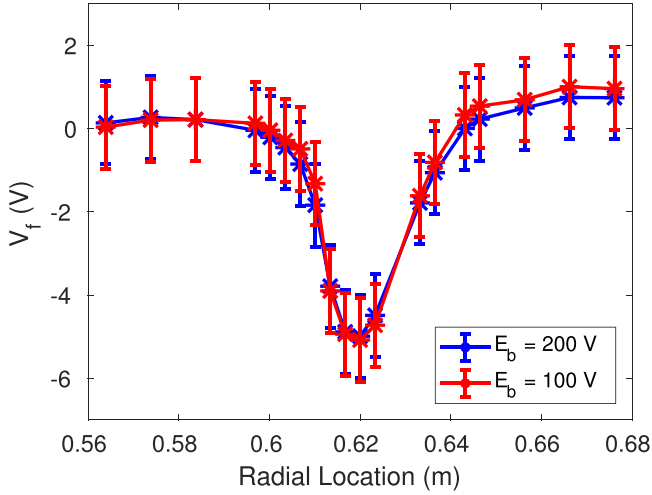


**Figure 6.** Radial floating potential profiles for  $E_b = 100$  (red) and 200 V (blue), when other key parameters such as the beam current  $I_m$ ,  $T_e$ , and  $n_e$  are similar. The two profiles are almost identical even with a different  $E_b$ , which support the hypothesis of weak beam-plasma interaction.

$1/2$  and  $\Delta T_{e\parallel}$ , respectively. Thus, the amount of  $V_f$  perturbation is

$$\Delta V_f \approx -\frac{2}{3}(3.3 + 0.5 \ln \mu) \frac{n_b}{n_e} E_b. \quad (7)$$

Equation (3) can be rewritten as

$$\Delta V_f = \frac{kT_e}{e} \ln \left[ 1 - \exp \left( \frac{1}{2} \frac{2n_b}{\pi n_e} \sqrt{\frac{2m_i e E_b}{m_e k T_e}} \right) \right]. \quad (8)$$

Under typical experimental conditions of  $T_e \sim 5$  eV,  $E_b = 200$  V, and  $\mu = 4$  (helium plasma), equations (7) and (8) give comparable estimates of  $\Delta V_f$ , which means that the local heating of electrons may result in the observed perturbation in  $V_f$ .

Since the two equations have a different dependence on  $E_b$ , it is possible to check which one is correct by varying  $E_b$  with the same beam current ( $I_m$ ), electron temperature ( $T_e$ ), and background density ( $n_e$ ). For the case of the weak beam-plasma interaction (equation (8)),  $\Delta V_f$  has a weak, if any, dependence on  $E_b$ , as  $n_b$  scales linearly with  $I_m/\sqrt{E_b}$ . For the case of strong beam-plasma interaction (equation (7)),  $\Delta V_f$  is larger with a larger  $E_b$ .

Figure 6 shows radial  $V_f$  profiles for two different values of  $E_b$ , when other key parameters are very similar; for  $E_b = 200$  V, when  $I_m = 0.41$  A,  $T_e = 5.3$  eV, and  $n_e = 1.8 \times 10^{12}$  cm $^{-3}$ , while  $I_m = 0.40$  A,  $T_e = 5.2$  eV, and  $n_e = 1.9 \times 10^{12}$  cm $^{-3}$  for  $E_b = 100$  V (red curve). The two profiles are almost identical, even though the  $E_b$  value is different. Together with the negligible broadening, these profiles support that the beam-plasma interaction is not strong enough to thermalize the electron beam while it travels about 0.20 m.

Figure 7 demonstrates the consistency of equations (3)–(5). This was done by using the  $\Delta V_f$  perturbation at  $R = 0.62$  m to estimate what the emitted current from the filament should be.

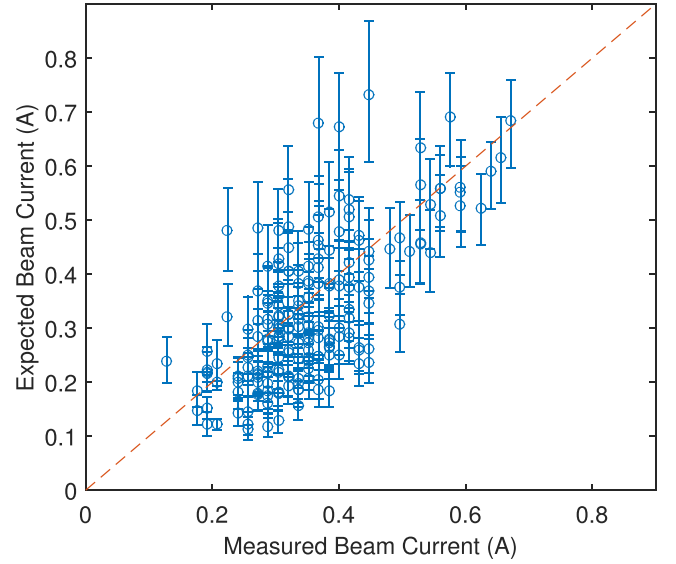


**Figure 7.** Comparison of the measured  $I_m$  to the calculated  $I_m$  given our averaged  $\sigma_R$  and  $\sigma_\theta$ . In order to quantify the consistency of equations (3)–(5) and of our determined effective widths, we have used the  $\Delta V_f$  perturbation at  $R = 0.62$  m to estimate what the emitted current from the filament should be. Each point is obtained from 50 discharges at four different discharge times (550, 650, 750, and 950  $\mu$ s). Errors in the expected value originates from the uncertainty in the measured  $n_e$ ,  $T_e$ ,  $\sigma_R$  (effective beam width), and from the uncertainty in determining  $\Delta V_f$  from the radial floating potential profile. The dashed line is the identity line, not a fit to data, but its correlation with the data is indicated by a reduced  $\chi^2$  value of 1.416.

This data was obtained from 50 discharges at four different times (550, 650, 750, and 950  $\mu$ s). The range of  $n_e$  and  $T_e$  is  $1\text{--}10 \times 10^{12}$  cm $^{-3}$  and 3–5 eV, respectively. Overall, the measured  $I_m$  agrees well with the expected  $I_m$  from equations (3)–(5) even with unquantified uncertainties such as the spatial separation of the Langmuir probe from the filament and probe array which affects  $n_e$  and  $T_e$  measurements, background electric fields and fluctuations, and the effects of the electron beam versus the biasing of the field lines by the filament. This indicates that effects from those uncertainties are not significant. The dashed line is the identity line, not a fit to data. The vertical error bars for the expected beam current comes mostly from uncertainties in  $n_e$  and  $T_e$  measurements, which are typically 5% for this condition. The uncertainty in the effective beam width,  $\sigma$  is also taken into account, which is 3%. This uncertainty is determined by the standard deviation of the measured  $\sigma$ . The vertical error bars for the measured  $\Delta V_f$  comes from the uncertainty in determining  $\Delta V_f$  from the radial floating potential profile, which varies shot by shot.

## 5. Conclusion

The results presented here suggests a new way of tracing a field line in a high density plasma, where the conventional tracing method by detecting light from the electron beam is not viable. We demonstrate that the presence of the electron



beam can be detected by measuring the floating potential after traveling about 0.20 m along the magnetic field. Moreover, there is no sign of noticeable broadening of the beam. These results prove that field line mapping in a high density plasma, in principle, can be achieved with a 2D or 3D mesh of floating potential probes. In addition, the stochasticity of the field line can be also determined with a 2D mesh of floating potential probes. If the beam width is observed to broaden far from the filament, one source of this broadening might be a stochastic magnetic field.

Possible effects from the two-stream instability [14–16] on the initial beam velocity must be discussed. The applicability of this method with a longer traveling distance may be limited by the broadening of the injected beam caused by high frequency instabilities as well as cross-field current driven by lower hybrid waves [17]. Even with instabilities, field line tracing by the floating potential measurement may be still possible as long as the electron beam is not significantly broadened. The dependence of the beam radius on the traveling distance is a future research topic and this future work will be crucial for the ultimate use of this diagnostic, which is determining the complex local 2D/3D magnetic geometry for studies of reconnection.

The floating potential profile also provides important information on the spatial profile of beam electrons, which suggests another application. The precise measurement of the 2D electron current density profile from an electron gun, for example, can be achieved by measuring 2D profiles of the floating potential in front of the electron gun with a background plasma. With the known beam velocity, this information can be easily converted to 2D profiles of the electron beam density [18]. This is a large advantage, since the floating potential measurement does not require complex electronic circuits, compared to the Langmuir probe measurement.

## Acknowledgments

This work is supported by the DOE contract No. DE-AC0209CH11466. The authors thank R Cutler and Chris Brunkhorst for their technical support. Data used for this manuscript is available in the DataSpace of Princeton University (<http://arks.princeton.edu/ark:/88435/dsp01x920g025r>).

## ORCID iDs

Jongsoo Yoo  <https://orcid.org/0000-0003-3881-1995>

## References

- [1] Colchin R J *et al* 1989 Electron beam and magnetic field mapping techniques used to determine field errors in the ATF torsatron *Rev. Sci. Instrum.* **60** 2680–9
- [2] Drewelow P, Bräuer T, Otte M, Wagner F and Werner A 2009 Three-dimensional photogrammetric measurement of magnetic field lines in the wega stellarator *Rev. Sci. Instrum.* **80** 123501
- [3] Lazerson S A, Otte M, Bozhenkov S, Biedermann C, Pedersen T S and the W7-X Team 2016 First measurements of error fields on W7-X using flux surface mapping *Nucl. Fusion* **56** 106005
- [4] Yamada M, Kulsrud R and Ji H 2010 Magnetic reconnection *Rev. Mod. Phys.* **82** 603–64
- [5] Yamada M, Ji H, Hsu S, Carter T, Kulsrud R, Bretz N, Jobes F, Ono Y and Perkins F 1997 Study of driven magnetic reconnection in a laboratory plasma *Phys. Plasmas* **4** 1936–44
- [6] Yoo J, Yamada M, Ji H, Jara-Almonte J and Myers C E 2014 Bulk ion acceleration and particle heating during magnetic reconnection in a laboratory plasma *Phys. Plasmas* **21** 055706
- [7] Chen S-L and Sekiguchi T 1965 Instantaneous direct-display system of plasma parameters by means of triple probe *J. Appl. Phys.* **36** 2363–75
- [8] Chan L Y and Stenzel R L 1994 Beam scattering and heating at the front of an electron beam injected into a plasma *Phys. Plasmas* **1** 2063–71
- [9] Lefebvre B, Chen L-J, Gekelman W, Kintner P, Pickett J, Pribyl P, Vincena S, Chiang F and Judy J 2010 Laboratory measurements of electrostatic solitary structures generated by beam injection *Phys. Rev. Lett.* **105** 115001
- [10] Hutchinson I H 2005 *Principles of Plasma Diagnostics* 2nd edn (Cambridge: Cambridge University Press)
- [11] Miyano R, Izumi S, Kitada R, Fujii M, Ikezawa S and Ito A 1996 Verification of sheath potential of processing plasma in an electron-beam-excited plasma apparatus using a current balance equation *Japan. J. Appl. Phys.* **35** 2427
- [12] Yoo J, Yamada M, Ji H, Jara-Almonte J, Myers C E and Chen L-J 2014 Laboratory study of magnetic reconnection with a density asymmetry across the current sheet *Phys. Rev. Lett.* **113** 095002
- [13] Van Compernelle B and Morales G J 2017 Avalanches driven by pressure gradients in a magnetized plasma *Phys. Plasmas* **24** 112302
- [14] Bailey V A 1948 Plane waves in an ionized gas with static electric and magnetic field present *Aust. J. Sci. Res. A* **1** 351
- [15] Pierce J R and Hebenstreit W B 1949 A new type of high-frequency amplifier *Bell System Tech. J.* **28** 33
- [16] Haeff A V 1949 A novel method of generation and amplification of microwave energy *Proc. IRE* **37** 4
- [17] Yamada M and Owens D K 1977 Cross-field-current driven lower-hybrid instability and stochastic ion heating *Phys. Rev. Lett.* **38** 1529–32
- [18] Miyano R, Izumi S, Kitada R, Fujii M, Ikezawa S and Ito A 1997 Influence of electron beam on profile of sheath potentials in electron-beam-excited plasma apparatus *Plasma Sources Sci. Technol.* **6** 551